Closed-Loop Vectoring Control of a Turbulent Jet Using Periodic Excitation

Article *in* Journal of Propulsion and Power · July 2003

DOI: 10.2514/2.6153

4 authors, including:

Kelly Cohen
University of Cincinnati
214 PUBLICATIONS **1,035** CITATIONS
SEE PROFILE

Avraham Seifert
Tel Aviv University
133 PUBLICATIONS **2,486** CITATIONS
SEE PROFILE

JOURNAL OF PROPULSION AND POWER
Vol. 19, No. 4, July–August 2003

Closed-Loop Vectoring Control of a Turbulent Jet Using Periodic Excitation

D. Rapoport,* I. Fono,† K. Cohen,‡ and A. Seifert§
Tel-Aviv University, 69978 Tel-Aviv, Israel

Closed-loop control strategies were studied experimentally at low Reynolds and incompressible Mach numbers using periodic excitation to vector a turbulent jet. Vectoring was achieved by attaching a short, wide-angle diffuser at the jet exit and introducing periodic excitation from a slot covering one quadrant of the circumference of the round turbulent jet. Closed-loop control methods were applied to transition quickly and smoothly between different jet deflection angles. The frequency response of the zero-mass-flux piezoelectric actuator was flat to about 0.5 kHz, but the jet responds up to 30–50 Hz only. This is still an order of magnitude faster than conventional thrust vectoring mechanism. System identification procedures were applied to approximate the system's transfer function. A linear controller was designed that enabled fast and smooth transitions between stationary deflection angles and maintained desired jet vectoring angles under varying system conditions. The linear controller was tested over the entire range of available deflection angles, and its performance is evaluated and discussed.

Nomenclature

A_{jet}	=	jet cross-sectional area, $\pi D^2/4$
A_{slot}	=	active excitation slot area, $\pi h D/4$
$C_{p,\text{cav}}$	=	actuator's cavity pressure coefficient, $P_{\text{cav,mean}}/\rho U_e^2$
C_μ	=	periodic excitation momentum coefficient, $J'/(\rho A_{\text{jet}} U_e^2)$
D	=	jet diameter, 39 mm
F^+	=	reduced frequency, fL/U_e
f	=	excitation frequency, Hz
h	=	excitation slot width, 1 mm
J'	=	periodic momentum at slot exit, $\rho A_{\text{slot}} u'^2_{\text{slot}}$
L	=	distance from jet exit to diffuser exit, measured along diffuser wall
$P_{\text{cav,lpf}}$	=	low-pass filtered cavity pressure, Pa
$P_{\text{cav,mean}}$	=	mean of actuator's cavity pressure, Pa
p	=	gauge pressure, Pa
p'	=	root mean square of pressure fluctuations, Pa
s	=	complex variable of the Laplace transform, $\sigma + j\omega$
t	=	time, s
U	=	jet mean velocity, m/s
u'	=	root mean square of the velocity fluctuations, m/s
x	=	axial direction, 0 at jet exit and diffuser inlet, mm
x_{is}	=	imaginary source of deflected jet, $-D/2$, mm
y	=	horizontal direction, 0 at jet centerline, mm
z	=	vertical direction, 0 at jet centerline, mm
z_c	=	jet center of linear momentum measured at $x = D$, $y = 0$, mm
δ	=	jet deflection angle, deg **arctan**$[z_c/(-x_{\text{is}} + D)]$, deg
$\bar{\delta}$	=	mean jet deflection angle of a step change, deg
ζ	=	damping ratio of transfer function pole
λ	=	time constant of internal model controller (IMC)
ρ	=	density of air
τ_n	=	time-constant of transfer function pole, s
τ_z	=	time-constant of transfer function zero, s
ω	=	radial frequency, $2\pi f$, rad/s

Subscripts

c	=	cutoff
cav	=	actuator's cavity
diff	=	diffuser wall
e	=	conditions at jet exit
slot	=	condition at slot exit

Received 16 September 2002; revision received 3 February 2003; accepted for publication 7 February 2003.

*Graduate Student, Department of Fluid Mechanics and Heat Transfer, Faculty of Engineering.
†Consultant, Department of Fluid Mechanics and Heat Transfer, Faculty of Engineering.
‡Israeli Defence Forces (IDF) Officer.
§Senior Lecturer, Department of Fluid Mechanics and Heat Transfer, Faculty of Engineering; Seifert@eng.tau.ac.il. Associate Fellow AIAA.

I. Introduction

CONVENTIONAL thrust vectoring systems are capable of significant jet deflection angles, enabling controlled flight at low speeds and high angles of attack resulting in super maneuverability. However, the complexity, weight, and thrust penalty associated with this added capability is large, and the slow response of the turning vanes or movable nozzle motivates the search for a simpler and faster alternative.[1–7] Active control of turbulent jets is not new. For several decades, researchers have introduced controlled excitation into the shear layers of laminar or turbulent jets, mainly to understand the underlying physics of large coherent structures and their role in jet mixing and noise generation.[8,9] Studies were conducted to explore the role of coherent structures in the control of boundary-layer separation.[10,11] Eventually, it was suggested[12] to combine the two approaches by attaching a short, wide-angle diffuser to the exit of a turbulent jet and to apply periodic excitation to the separated shear layer to promote reattachment of the jet to the diffuser walls. Controlling the entire circumference of the jet enhances its spreading rate, reduces the noise, and increases the thrust efficiency. Introducing the periodic excitation to a fraction of the jet circumference moves the entire jet toward the controlled diffuser sector. Therefore, the jet is deflected up to the same angle as the diffuser wall, instead of being just slowed down by it. It was further shown that the deflection angle is proportional to the magnitude of the excitation C_μ (Ref. 13). It was clearly demonstrated that the presence of the diffuser at the jet exit enhances the capability of the periodic excitation to vector the jet. Additional modes of excitation were found, and the optimal values of the most significant parameters were identified.[13] Initial transient response tests of the jet deflection as a result of applying step and impulse control inputs demonstrated that the jet responds on the order of 10–20 ms, (50–100 Hz) and, more important, that the response is not sensitive to the jet speed

(and Reynolds number). The response has several common features with second-order, underdamped systems.[13] Similar responses were previously seen in external aerodynamic applications of active separation control using periodic excitation.[14,15]

The present investigation uses the existing jet facility[13] to perform a closed-loop active flow control experiment, with the aim of smooth and rapid transition from one state, that is, jet deflection angle, to another.

The experiment was first focused on the system's static and dynamic responses, including linearity tests. It was continued with a search for a simple and reliable method for real-time detection of the system's state. Initially, a single hot-wire probe was used to measure the shear layer velocity variations as an indication of the jet deflection angle. Additional measuring techniques subsequently used were steady and unsteady diffuser surface and actuator's cavity pressures. The primary control input was the amplitude of the cavity pressure fluctuations, with a flat frequency response up to about 0.5 kHz.

MATLAB® and SIMULINK® simulations were used to assist in the design and optimization of the controller, and dSPACE™ digital signal processor (DSP) control hardware and real-time software were used to perform the experiments.

The paper includes discussions of the static characterization experiments of the actuators and jet response (Sec. III.A), development of a dynamic model for the response of the turbulent jet (Sec. III.B), and design of the closed-loop control system, closed-loop control of the turbulent jet, and operation outside the design envelope (Sec. III.B.3).

II. Experiment Setup

The jet facility consists of a dc fan connected to a 76.2-mm-diam settling chamber, leading to a 3.15:1 contraction that is followed by a straight aluminum pipe with an inside diameter of 38 mm and an outside diameter of 40 mm. The thickness of the pipe wall at the jet exit was machined to bring it gradually down to 0.5 mm, to reduce the gap between the jet flow and the excitation slot, that is, $D = 39$ mm (Figs. 1a and 1b). A segmented slot, 1 mm wide, surrounds the jet. The excitation was introduced through the slot surrounding the upper 90 deg of the jet circumference (Fig. 1b). Trip grit (number 36) was placed inside the aluminum pipe, 200 mm from the jet exit, to ensure that the flow at the jet exit was turbulent. The jet exit velocity was determined by the static pressure in the jet plenum.

A short ($L = 0.58D$), wide-angle ($\phi = 30$ deg) diffuser was attached to the jet exit. In previous publications,[13] the effects of various diffuser spreading angles and length were discussed, but here the shortest yet effective diffuser tested to date was used.

An unsteady pressure transducer was installed in the diffuser wall, 2 mm from the jet exit in line with the active segment of the actuator, to measure the dynamic response of the jet vectoring. The transducer was mounted inside a miniature cavity that was connected through a 0.5-mm-diam orifice to the flow exposed side of the diffuser.

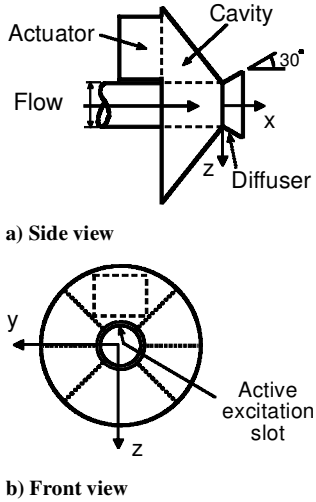

Fig. 1 Schematic description of the experimental setup with the diffuser (a) and without the diffuser (b).

A zero-mass-flux piezoelectric actuator, which resonated at 725 Hz, was used to generate the periodic excitation. The velocity fluctuations exiting the slot, u'_{slot}, were measured using a hot wire positioned at the slot exit, while $U_e = 0$. An unsteady pressure transducer was mounted in the actuator's cavity to measure the static and dynamic cavity pressures. The p'_{cav} signal indicated the actuator's performance, whereas $P_{\text{cav,lpf}}$ (obtained using a fifth-order Butterworth low-pass filter with a 200-Hz cutoff) was used to close the control loop as will be discussed in Sec. III.A.2.

The jet velocity was measured by a hot wire that was calibrated at the jet exit, and data repeatability was often checked. Data were low-pass filtered with a third-order Butterworth filter ($f_c = 3.8$ kHz), and sampled at 8192 Hz using a 12-bit A/D converter. The frequency response of the hot wire and unsteady pressure transducer were better than 20 kHz. The hot wire was mounted on a three-axis traverse system. The velocities measured with the hot wire are accurate to within 2%. The hot-wire position, x, y, or z, is known to within ± 0.04 mm, the C_μ is accurate to within 15%, and δ estimates[13] are within ± 1 deg. All data presented were acquired at jet exit velocities between 10 and 14 m/s, resulting in Reynolds numbers between 2.5×10^4 and 3.5×10^4.

III. Discussion of Results

A. Static Response of the Plant

1. *Actuator Static Response*

Static testing of the actuator and actuator–flow interaction were performed to characterize its response and to establish its gain, offset, and linearity. These tests revealed that the resonance frequency of the actuator is around 725 Hz, and this frequency was used throughout the present investigation. The actuator was characterized using an unsteady pressure sensor installed inside the actuator's chamber (Fig. 1a) and simultaneously by a hot wire that was placed at the slot communicating the actuator and the jet flow. A linear relationship was established between the excitation voltage provided to the actuator and the resulting p'_{cav} that is advantageous from the control aspect. The measured p'_{cav} was used as the primary control input instead of the excitation voltage because it compensates for variations in the actuator's performance and it enables maintaining system performance, regardless of the actuator's health (as long as sufficient control authority is maintained).

The u'_{slot} was measured by a hot wire in the absence of jet flow. Care was taken to align the hot wire in the actuator's slot such that the blowing and suction related peak velocities were identical and the resulting velocity signal matched an ideally rectified sine wave. The maximum output of the actuator was about 18 m/s, with the linear relationship $u'_{\text{slot}}\ \text{m/s} = 0.036 p'_{\text{cav}}$ Pa. The effect of the jet exit velocity or the presence of a diffuser changes the u'_{slot} by less than 5% (Ref. 13). Although it was established that the u'_{slot} (or C_μ) is the leading flow control input, the current experiment used p'_{cav} as the primary input due to its linear relationship with u'_{slot} and the ability to monitor it when the hot wire was removed.

2. *Jet Static Response*

The static jet flow response to the control input was measured when a quarter of the jet circumference was excited periodically with the wide-angle diffuser present (Fig. 1a). The result of the excitation was a gradual spreading and vectoring of the jet toward the excited shear layer, that is, negative z direction, at angles up to 10 deg for C_μ of up to 7% (Ref. 16), in agreement with previous data.[13] Jet deflection angles were estimated from a single vertical velocity profile measured at $x = D$, $y = 0$, and the imaginary source of the jet was always taken at $x_{\text{is}} = -0.5D$ (Ref. 13). It was found that the jet deflection angle is almost linearly dependent on p'_{cav} (Fig. 2), which is also linearly related to u'_{slot}. The latter and, therefore, also p'_{cav} are proportional to $\sqrt{(c_\mu)}$. This finding indicates that p'_{cav} could be used as a convenient control input.

The data presented in Fig. 2 were acquired 15 months apart and provide an indication of the data repeatability. Furthermore, between

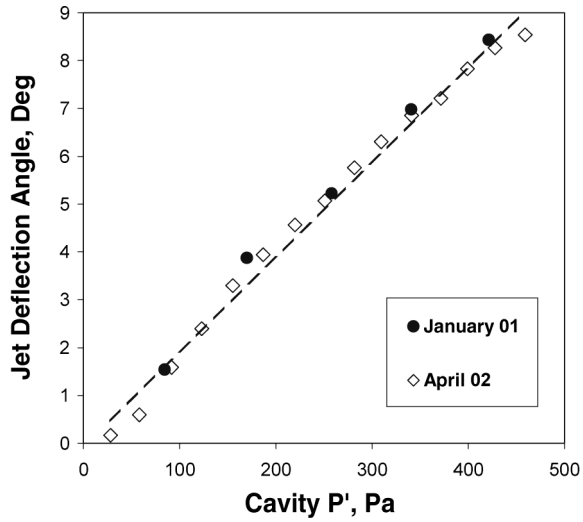

Fig. 2 Jet deflection angle vs actuator's cavity pressure fluctuation level also showing data repeatability.

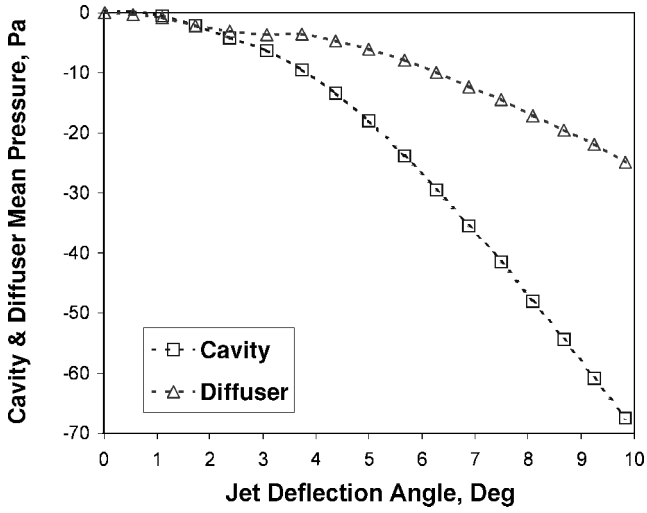

Fig. 3 Actuator's cavity and diffuser mean pressure ρ to obtain a desired jet deflection angle at U_e = 12 m/s.

the acquisition of the first and second data sets, one of the multiple piezoactuators driving the cavity was damaged. However, because the control input parameter was p'_{cav}, it resulted in only increased excitation voltage, with no effect on δ.

The next step in the static jet characterization was a search for sensor type and optimal placement for "closing the loop." It is clear that an intrusive velocity sensor such as a hot wire cannot be used beyond preliminary laboratory experiments, and therefore, it was used only as an indicator of the jet state. Diffuser skin friction measured by hot films is another possibility that was rejected due to the assumption that the jet does not fully reattach to the diffuser, and therefore, significant changes in skin friction are not expected. The next logical option to consider was the diffuser pressure. It is a local quantity, but it is directly related to the forces acting on the diffuser and jet. Therefore, an unsteady pressure sensor was also placed on the diffuser wall (in addition to the one installed in the actuator's cavity), 2 mm from the active excitation slot. Static tests revealed that $P_{\text{diff,mean}}$ is reduced as the jet is vectored (Fig. 3). However, a similar and even stronger response was measured in $P_{\text{cav,mean}}$. The reduced pressure is generated by the curvature of the jet streamlines as it turns closer to the diffuser wall (or vise versa), but the suction peak has to be the strongest at the corner, that is, where the actuator slot is located. The finding that $P_{\text{cav,mean}}$ is stronger, while the sensor placed at the diffuser wall also exhibits a high level of fluctuations at the actuator's resonance frequency (725 Hz), makes the use of the diffuser sensor redundant. In addition, the sensor placed at the actuator's cavity is better protected from external hazards. Therefore, it was decided to use $P_{\text{cav,lpf}}$, as the primary indicator of the jet deflection angle (Fig. 3). The hot-wire velocity signal, just opposite the active slot at $x/D = 1$, was used as an indicator for the success of the control strategy. Clearly, the cavity pressure is a better and more convenient choice for positioning a sensor for closed-loop control purposes because it is nonintrusive and eliminates the need for at least two separate sensors: one to monitor the actuator and the other to sense the flow state. The actuator's cavity pressure is both statically and dynamically similar to the diffuser pressure, only the cavity signal is larger.

3. Effect of Jet Mean Exit Velocity

Certain jet flow control applications require constant jet deflection angle under varying operating conditions. Examples are thermal protection, industrial processing, chemical reactions, and pollutant dispersion in the atmosphere. To maintain a constant jet deflection angle, one needs to explore statically the effect of the jet exit velocity on the resulting jet deflection angle. Certainly, an additional sensor should be added to monitor the jet exit velocity by, as an example, measuring the static pressure in the jet plenum.

Experiments were conducted to determine the static δ by varying p'_{cav} at three levels of U_e. The data indicated that δ decreased as U_e increased for a constant level of p'_{cav}. However, when δ is plotted against p'_{cav}/U_e that is proportional to $\sqrt{(C_\mu)}$, the data coalesce to a single curve (Fig. 4). Although physically meaningful, C_μ is not a convenient control parameter. Still, it provides a guideline as to the required control methodology: Measure U_e, along with p'_{cav}, and use the ratio p'_{cav}/U_e as the control input. If the ambient pressure change divide also by ρ.

As an indicator for the jet deflection angle, we suggest to use $C_{p,\text{cav}}$. Figure 5 clearly shows that, when plotting $C_{p,\text{cav}}$ vs the required δ, the data collapse into a single curve for the three levels of U_e tested. Nevertheless, it is not a linear relationship. The curve in Fig. 5 was used to establish the correlation to derive the required $C_{p,\text{cav}}$ for a desired δ. Multiplying the result by U_e^2 provides the set-point for the closed-loop control system. Velocity profiles acquired when the controller maintained a fixed δ, regardless of variations of U_e, demonstrate the success of the selected approach.[16]

B. Dynamic Response of the Plant

1. Preliminary Actuator and Flow Dynamic Response

A dynamic characterization of the actuator revealed that its response, as measured by p'_{cav}, resembles a first-order system with a time constant of about 5 ms. It has been shown[16] that the current piezoactuator could reach steady state within 2–3 ms using a modified step input. However, it was found that the flow response resembles a second-order system with an initial inverse response and

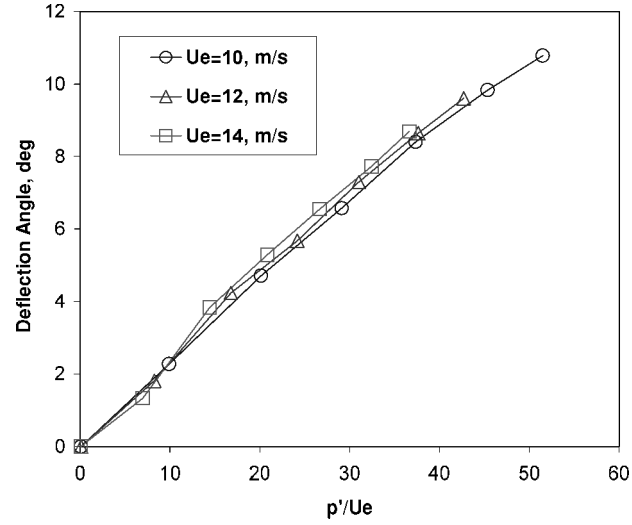

Fig. 4 Jet deflection angle for three mean jet exit velocities vs cavity pressure fluctuations divided by the mean jet exit velocity.

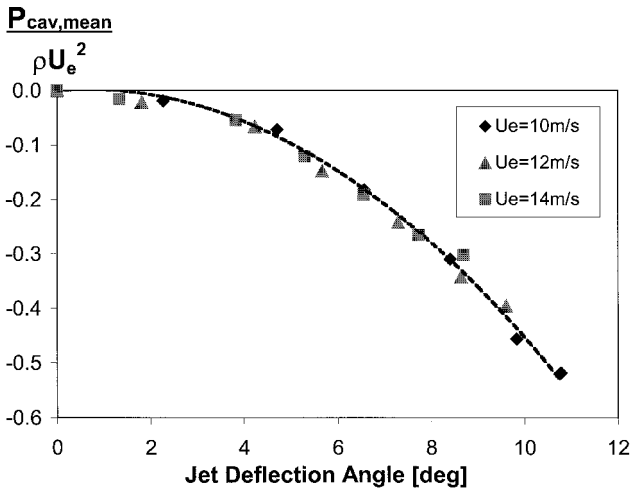

Fig. 5 Cavity pressure coefficient $C_{p,\mathrm{cav}}$ vs the jet deflection angle for three mean jet exit velocities.

an overshoot.[16] The inverse response is typical of a nonminimum phase system (system with a transmission zero at the right-hand-side half of the complex plane).[17] When the modified step input is used,[16] the severity of the inverse response increased, as did the magnitude of the overshoot. These undesired effects were accompanied by a small decrease in the rise time (defined as the time passed from the command to the first crossing of the setpoint). The conclusion drawn from this test was that one would need to use a more gradually evolving input signal, that is, rate limited, to smooth the undesired transients.

Even with the rate limiter (ramp of 20 ms), the flow response indicates that a 30–50 Hz frequency response could be achieved in real, full size systems (for a proportional increase in size and speed), which is an order of magnitude faster than conventional thrust vectoring and control surface frequency response.[16]

2. *System Identification of Jet Vectoring Using Frequency Sweep*

Linearization. The relationship between the jet deflection indicator $P_{\mathrm{cav,mean}}$ and the jet deflection is nonlinear (Fig. 3). To find a linear model of the plant, the first step is to establish an operating point and a range around which the response curve is approximately linear. The chosen operating point was $p'_{\mathrm{cav}} = 360$ Pa and the operating range from 250 to 465 Pa at $U_e = 12$ m/s (corresponding to $\delta = 7.2$, 6.3, and 8.5 deg, respectively). All subsequent experiments related to the identification of the plant were performed for this range of parameters.

Modeling. The purpose of dynamic modeling is to establish a mathematical description of the physical system (plant). Experimental modeling typically assumes an a priori form of the model and then uses available measurements to estimate the coefficient values that cause the assumed form to best fit the data. The assumed plant transfer function was $H(s) = B(s)/A(s)$, that is, a rational function of polynomials in s. The input to the plant was an amplitude modulated sine wave at 725 Hz, the resonance of the piezoactuator. The amplitude of the 725-Hz signal (without modulation) was statically adjusted to provide an excitation of $p'_{\mathrm{cav}} = 360$ Pa, the chosen operating point, resulting in a steady $\delta \approx 7$ deg (Fig. 2). The amplitude modulating (AM) signal was a swept sine (chirp) in the range 1–90 Hz with sweep time of 90 s [$\mathrm{AM}(t) = \lfloor 1 + 0.3 \sin(2\pi t + t^2) \rfloor \sin(2\pi 725 t)$].

Figure 6a shows the initial 2.5 s, and Fig. 7a shows the final 0.05 s of the AM signal. This frequency range was selected because the jet response at higher frequencies was significantly attenuated. Figures 6d and 7d present the hot-wire measured velocity response. The amplitude of the AM signal was adjusted to provide 30% modulation to cover a partial, linear operating range of the plant as mentioned earlier. The resulting excitation signal to the actuators

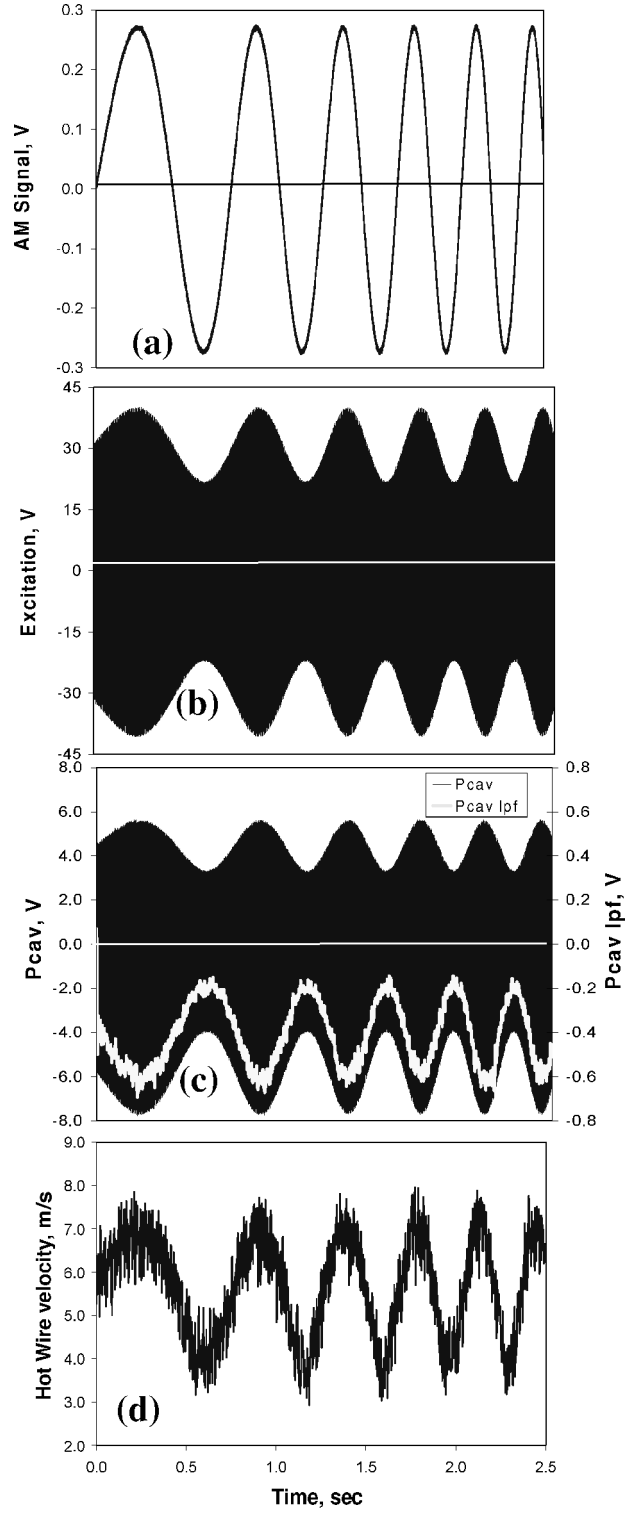

Fig. 6 AM chirp signal: a) initial 2.5 s, b) excitation signal to piezoactuators, c) resulting actuator's cavity pressure P_{cav} and its low-pass filtered part $P_{\mathrm{eav,lpf}}$ shown in light color, and d) hot-wire measured velocity [m/s].

is shown in Figs. 6b and Fig. 7b. Note that the 725-Hz excitation cannot be seen in the plot resolution of Fig. 6b.

Data acquisition. The input AM signal, together with the plant responses (P_{cav} and the hot-wire velocity at $x/D = 1$) were amplified, low-pass filtered with a third-order Butterworth filter ($f_c = 3.8$ kHz) and acquired at a sampling rate of 8192 Hz with a 12-bit A/D converter. The data were ensemble averaged over 10 realizations, sufficient to remove random noise from the P_{cav} signal

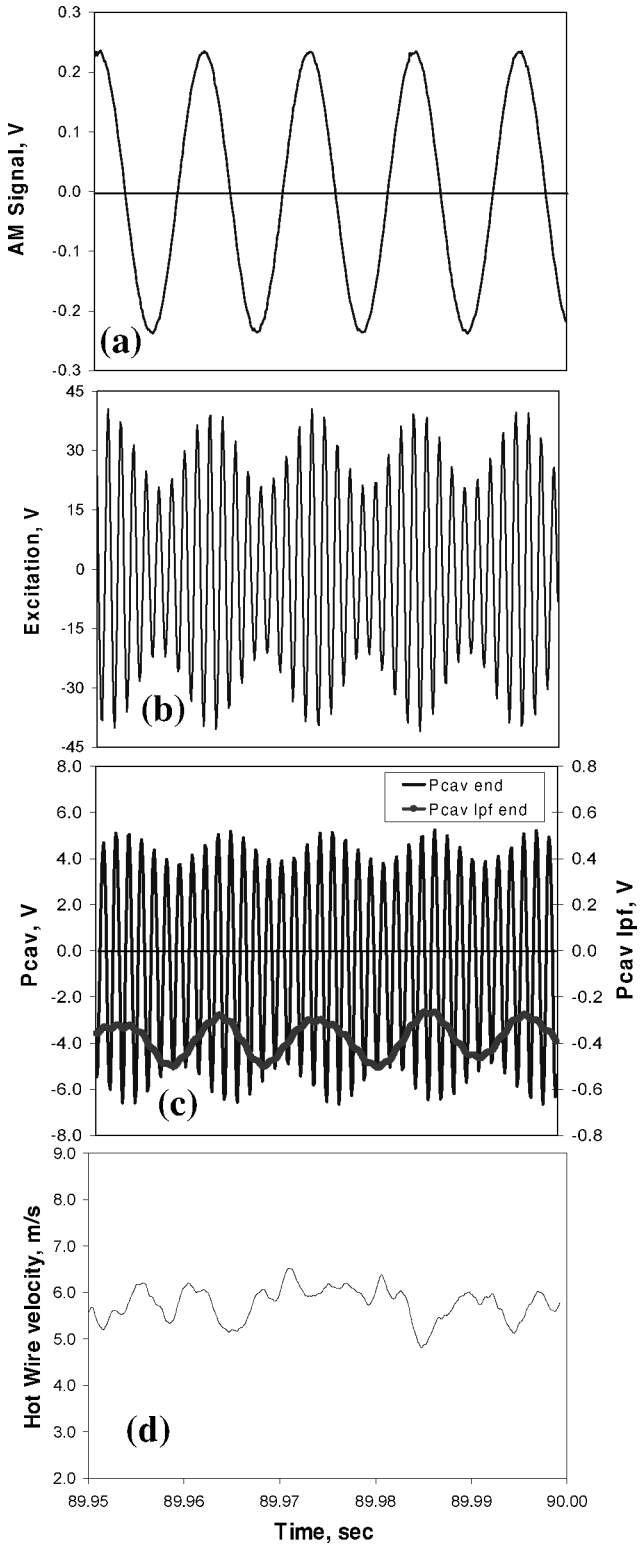

Fig. 7 AM chirp signal: a) final 50 ms, b) excitation signal to piezoactuators, c) resulting actuator's cavity pressure P_{cav} and its low-pass filtered part $P_{cav,lpf}$, and d) hot-wire measured velocity [m/s].

(Figs. 6c and 7c) but certainly not enough for the noisy turbulent jet velocity signal (Figs. 6d and 7d). However, the hot-wire signal was only used as an independent indicator for the jet deflection and not as a sensor for closed-loop operation. The hot wire was positioned at $x/D = 1$ at a point z in the shear layer such that $U = U_{max}/2$.

Figure 6d shows the initial 2.5 s of the hot wire signal with the AM signal operating, indicating that the jet closely follows the input signal, whereas Fig. 7d presents the final 0.05 s of the velocity data showing the lack of flow response to the AM signal at 90 Hz.

Figures 6c and 7c present the P_{cav} signal, showing the lack of symmetry, with a mean less than zero, indicating negative $P_{cav,lpf}$, which is a result of the varying jet deflection angle (corresponding the static tests, Fig. 3). Also note the inverse relationship between the time-dependent amplitude of the P_{cav} signal and $P_{cav,lpf}$, that is, the higher the magnitude of p'_{cav}, the more negative $P_{cav,lpf}$ becomes. This is due to larger jet deflection angle that caused increased acceleration around the jet-diffuser corner, lowering the local static pressure. The $P_{cav,lpf}$ is also plotted in Figs. 6c and 7c, with the ordinate on the right-hand side of those charts. Note that this ordinate is smaller than the left-hand-side ordinate by a factor of 10 and that $P_{cav,lpf}$ in Fig. 6c is indicated by a light color. Remembering that $P_{cav,lpf}$ is indicative of the δ (Fig. 3), one can note that for low modulating frequency, δ follows closely the amplitude of p'_{cav}. For high modulating frequency (Fig. 7c), the amplitude of $P_{cav,lpf}$ is significantly attenuated, and a phase shift of almost 180 deg develops between the input excitation and the resulting jet deflection angle. Approximately 80 deg of the phase lag is the result of the low-pass filter used. The additional 100-deg phase shift is physically reasonable because the jet with a time constant of about 10 ms develops an increasingly larger phase lag with increasing modulating frequency. In addition, the magnitude of the δ fluctuations is attenuated as the AM frequency increases. When the modulating frequency approaches 100 Hz, the jet will no longer follow the changes in the AM signal.

Data processing. The ensemble-averaged input stimulus and plant response signals were transformed to the frequency domain by a fast Fourier transform (FFT). Because the power spectral density of the input chirp signal is nonstationary, the FFT was computed from the complete time history record of length 737,280 points sampled at 8192 Hz. No block overlap or windowing was used. From the transformed data, only the relevant frequency components from 1 to 90 Hz were considered for modeling, corresponding to the frequency range of the input stimulus (AM signal). The FFT of the response signal divided by the FFT of the input AM signal is the measured complex plant frequency response $H(j\omega)$. The measured Bode plot of the plant is presented in Figs. 8a and 8b. The frequency response is flat with the -3-dB point (referenced to the response at 1 Hz, amplitude ratio of 0.707) at about 60 Hz. The phase lag between the AM signal and $P_{cav,lpf}$ is initially 180 deg, as shown in Figs. 6a–6c. It reaches 80 deg at 60 Hz, but part of this change is due to the Butterworth filter.

Transfer function. The plant transfer function was found from the complex frequency response $H(j\omega)$ by assuming a transfer function of the form $H(s) = B(s)/A(s)$ and numerically searching for the coefficients of $B(s)$ and $A(s)$ that best fit the data. The order of the numerator and denominator of the transfer function were arrived at by performing several iterations of the described procedure and choosing the orders that provided the best correspondence with both the magnitude and the phase of the plant frequency response. The resulting transfer function of the plant is

$$H_{plant}(s) = K \cdot \frac{\tau_z s - 1}{\tau_n^2 s^2 + 2\tau_n \zeta s + 1}$$

where

$$K = 0.773, \qquad \tau_z = 1.39 \times 10^{-3} \text{ s}$$

$$\tau_n = 1/2\pi f_n = 2.3 \times 10^{-3} \text{ s}$$

$$f_n = 69.2 \text{ Hz}, \qquad \zeta = 0.935$$

Figures 8a and 8b present the Bode plots of the plant. It demonstrates the good correspondence between the measured and modeled data. The form of the transfer function $H(s) = B(s)/A(s)$ assumes zero transport delay. If the measured signal has significant

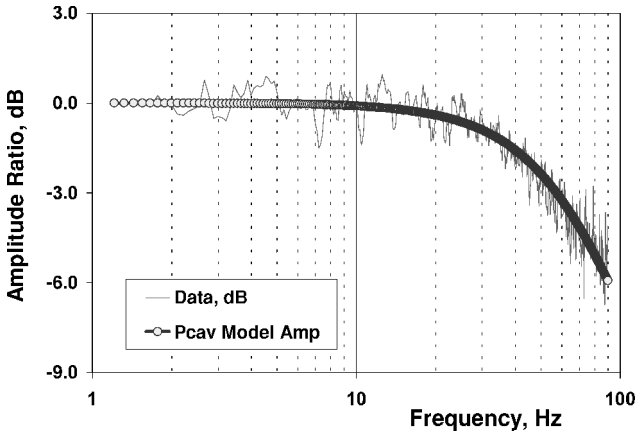

a) Normalized amplitude ratio

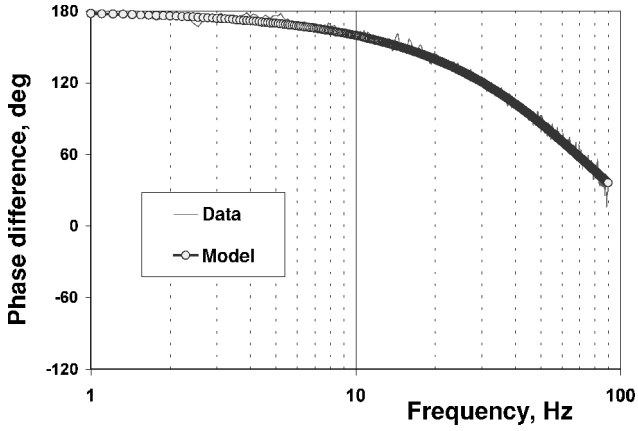

b) Phase lag

Fig. 8 Bode plot of $P_{\text{cav,lpf}}$ in response to AM signal.

delay, as in the case of the velocity signal measured at $x/D = 1$, the frequency-response data should be corrected before it can be modeled.[16]

3. *Implementation of the Closed-Loop Control*

Controller design and optimization. The controller was designed for the plant model described in Sec. II to meet several closed-loop performance criteria, for example, fast rise-time, minimal inverse response, minimal overshoot, and zero steady-state error, for a step change in the input, that is, the required δ. Furthermore, the controller should perform well under a wide range of operating conditions, including random noise, changing jet exit velocity, and partial loss of actuator output. In other words, the controller should be robust. To achieve these goals, three controller configurations were investigated: proportional, integral, derivative (PID); PI with rate feedback; and internal model control (IMC).

The following text contains description of the third controller only; a description of the first two may be found in Ref. 16.

IMC. A fundamental problem controllers have to overcome is the inherent uncertainty in plant models. If the plant model were perfect, that is, matched the plant under all operating conditions, closed-loop control would not be needed, and the transfer function of the controller would simply be the inverse of the plant model, resulting in an ideal step response. However, real systems are impossible to model perfectly, and therefore, when attempting to control the plant, feedback is needed to take into account the model inaccuracies.[18]

In the IMC configuration, the controller's output simultaneously enters the plant and its model (Fig. 9). To account for model uncertainty, the difference between the responses of the plant and the model is used as the feedback signal. The input to the controller is the difference between this feedback signal and the required setpoint.

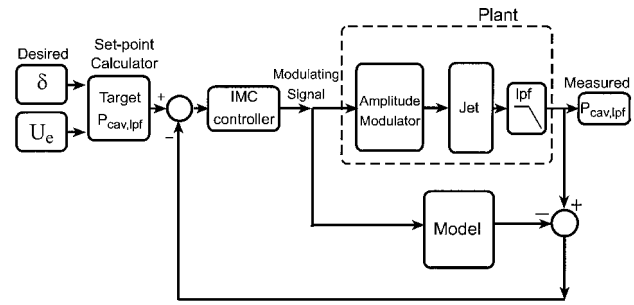

Fig. 9 Complete closed-loop control system.

The transfer function of the controller is the inverse of the model, multiplied by an additional real pole at $-1/\lambda$, where λ is the effective IMC controller time constant. The multiplicity of this pole, n, is the difference between the order of the model's denominator and numerator. The IMC controller should be based on a reasonably accurate plant model. If that is not the case, the advantage of the IMC controller is significantly diminished.

In the present investigation, the plant's model included a zero in the right-half of the complex plane; therefore, the model cannot be inverted as is because a right-hand side unstable pole always results. To solve the latter problem, the model was partitioned into its minimum-phase, that is, without the right-half plane zero, and its nonminimum-phase components as follows:

$$H_{\text{plant}}(s) = \frac{P_{\text{cav,lpf}}(s)}{\text{AM}(s)} = P_A(s) \cdot P_M(s)$$

where

$$P_A(s) = \frac{-s + 716.85}{s + 716.85}, \qquad P_M(s) = \frac{s + 716.85}{-0.005s^2 - 4s - 927.58}$$

and $P_A(s)$ is the nonminimum-phase part of the model that is also called the all pass part; $|P_A(s)| = 1$ for all ω. $P_M(s)$ is the minimum-phase part of the model, and therefore, it is invertible.

Finally, the IMC controller transfer function was defined by

$$H_{\text{IMC}}(s) = \frac{1}{\lambda s + 1} \cdot \frac{1}{P_M(s)} = \frac{-0.005s^2 - 4s - 927.58}{\lambda s^2 + (716.85\lambda + 1)\, s + 716.85}$$

The advantage of the IMC controller is its simplicity: Only one parameter, λ, needs to be tuned to achieve optimal step response; otherwise, its performance is equivalent to a PID controller.

Real-time implementation and testing. Once the simulation results met the performance criteria, the SIMULINK® model of the controller was compiled and downloaded into the DSP board. The excitation signal to the plant's Piezo actuators was provided by one of the 14-bit D/A converter channels of the DSP board. A 16-bit A/D converter channel of the same board acquired in real time the output signal of the unsteady actuator's cavity pressure sensor. The minimum rate used for closed-loop control was 10 kHz. The $P_{\text{cav,lpf}}$ was used as the primary indication of the jet deflection angle, that is, the plant output. Figure 9 shows the diagram of the complete closed-loop system.

Monitoring the real-time closed-loop performance of the plant was then performed. The same work environment was used for online tuning of the controller parameters to achieve optimal performance. Concurrently the DSP board acquired the relevant time–history data that were saved for postprocessing.

Selection of the IMC controller time constant. The main advantage of the IMC controller is that, to achieve optimal closed-loop performance, only one parameter, λ, should be tuned. Figures 10a and 10b present the closed-loop step response of the controlled variable $P_{\text{cav,lpf}}$ and the velocity signal for three different λ. The velocity was measured at $x/D = 1$ at a point z in the shear layer such that

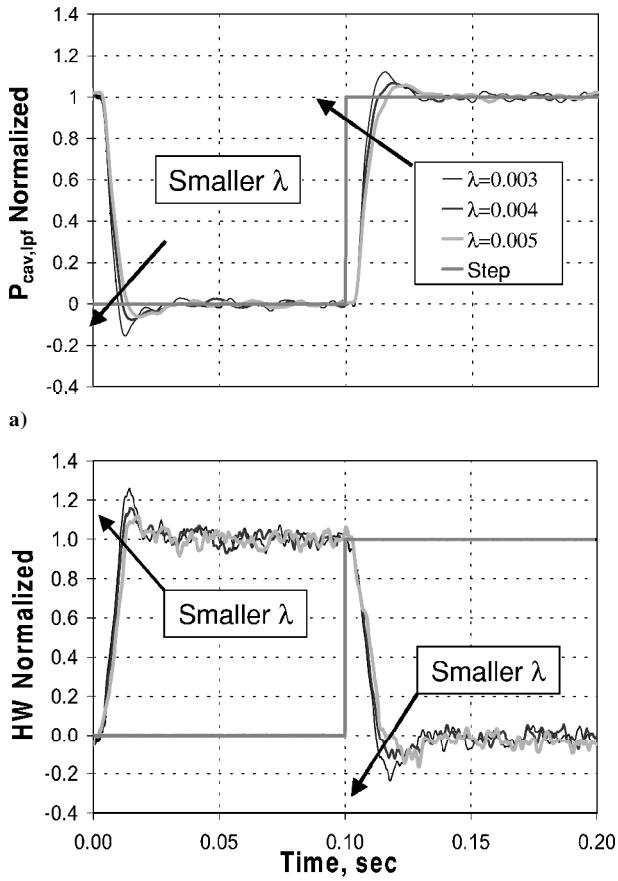

Fig. 10 Selection criteria for the IMC controller time constant λ: a) $P_{cav,lpf}$ and b) hot-wire measured velocity at $x/d = 1$ opposite actuator.

$U = U_{max}/2$ while the mid range p'_{cav} was 360 Pa. Note the linearity of the responses, inasmuch as the low-to-high and high-to-low jet deflection transitions are almost identical regardless of λ. An additional important feature of the IMC controller is that, even though there is a certain dead time, only minimal inverse response was observed. This is partly due to the rate-limiting effect of the controller's time constant and partly to the low-pass filter in the loop.

The data presented in Fig. 10 are also an indication that, when operating within the linear range of the static flow response curve (Fig. 3), the designed IMC controller performs well. The arrows indicate the direction of the decreasing time constant. Based on these results and limiting the overshoot to 10%, $\lambda = 0.004$ was selected. The system settles to within 5% of its final value in about 20 ms, and there is no steady-state error. If a faster response is deemed essential, a smaller λ could have been used, with the penalty of a larger overshoot and a stronger inverse response. Note the inverse relationship between the cavity pressure and velocity responses.

Closed-loop plant response. The closed-loop frequency response of the plant was measured by exciting the system with a swept sine signal using frequencies between 1 and 90 Hz. The measured and modeled Bode plots of the closed-loop system with IMC controller are shown in Figs. 11a and 11b. The bandwidth of the closed-loop system, is approximately 50 Hz, not much different from that of the plant (also shown in Fig. 11). The closed-loop amplitude ratio indicates a slightly underdamped system, commensurate with the 10% overshoot mentioned before. The phase lag at 50 Hz is about 140 deg. The measured and modeled step responses of the closed-loop system are shown in Fig. 12. The excellent agreement speaks for itself.

The main benefits of the current implementation of the IMC controller and the selected λ are in reducing the inverse response and

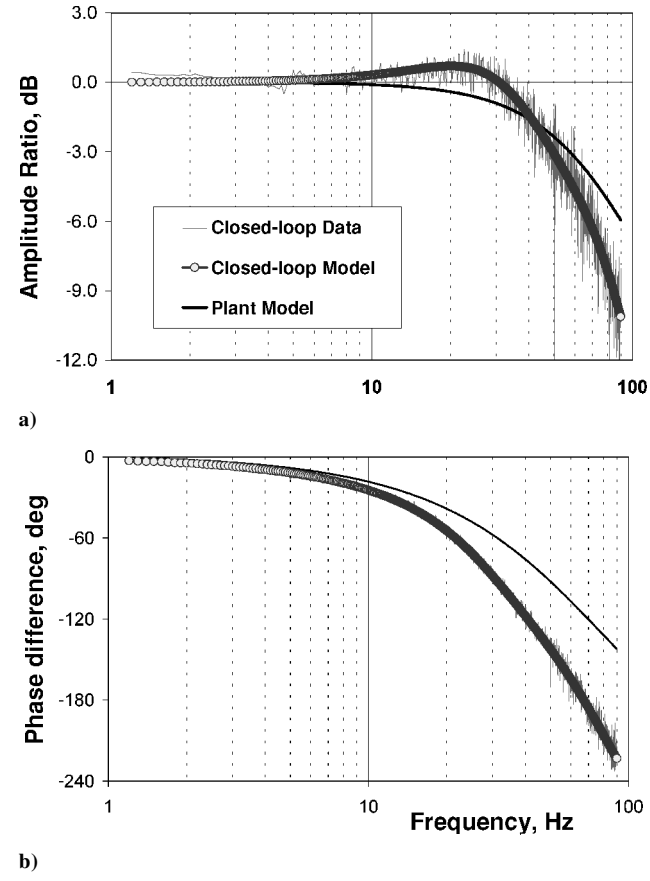

Fig. 11 Measured closed loop data and its model, compared to plant model: a) amplitude ratio and b) phase lag.

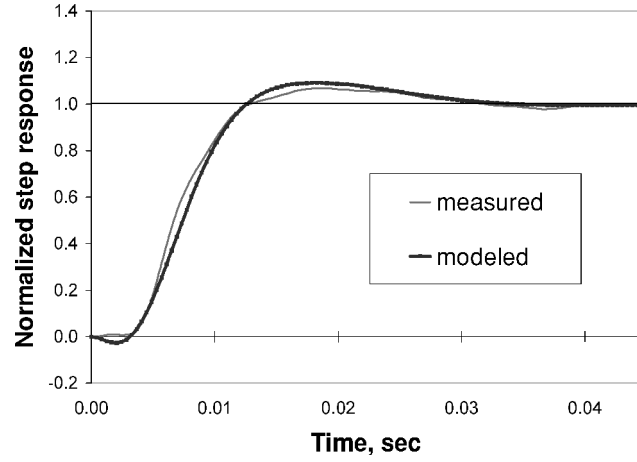

Fig. 12 Modeled and measured closed-loop step response.

ensuring zero steady-state error and not necessarily a wider bandwidth. The latter task could be achieved by a selection of a smaller λ that perhaps should be accompanied by a higher cutoff frequency low-pass filter for the cavity pressure signal used as a sensor for the jet deflection angle.

Operation outside the design envelope. A linear controller functions less than optimally outside the linear range of the system. The IMC controller was designed to operate in the jet deflection range of 5–9 deg, where the static sensitivity of the $P_{cav,lpf}$ to δ is close to linear (Fig. 3). Nevertheless, operation at a wider range of jet deflection angles, outside the linear range, was also tested, to quantify the degradation in the controller's performance and to determine if a more sophisticated control methodology should be attempted.

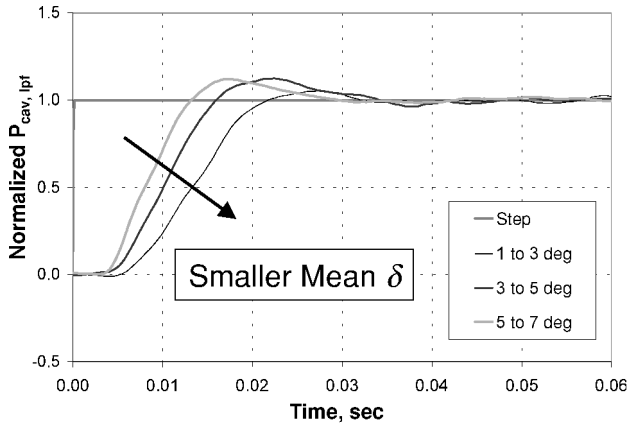

Fig. 13 Closed-loop 2-deg step response for increasing δ (inverted $P_{cav,lpf}$).

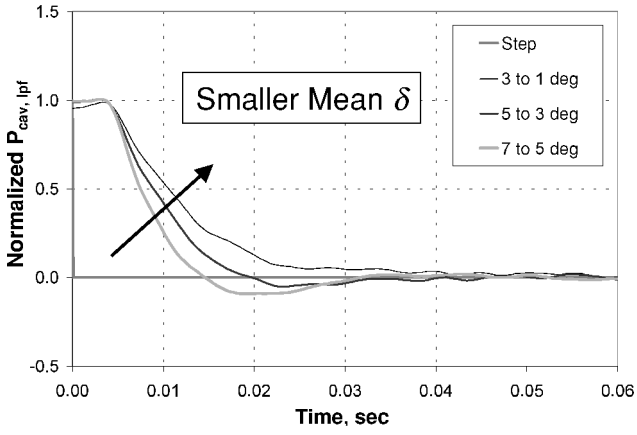

Fig. 14 Closed-loop 2-deg step response for decreasing δ (inverted $P_{cav,lpf}$).

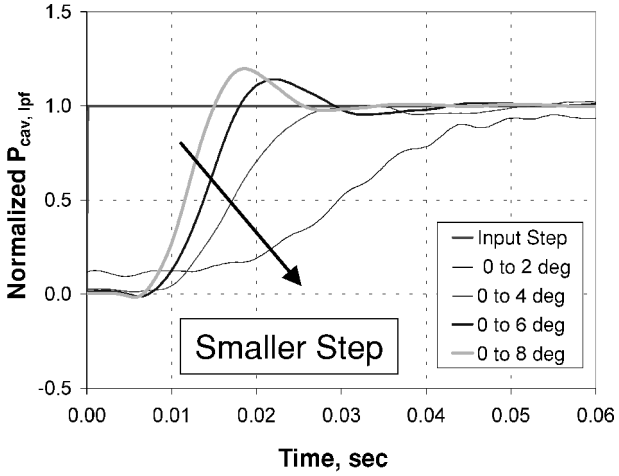

Fig. 15 Closed-loop jet deflection step, δ increasing from zero (inverted $P_{cav,lpf}$).

Figure 13 presents the response of $P_{cav,lpf}$ to a 2-deg step increase in δ. Figure 14 presents data for the same step size but for decreasing δ. While operating inside the design space, that is, 5–9 deg, the jet response is quick and smooth. It settles to the new state within 25–30 ms. As $\bar{\delta}$ decreases, the response becomes more sluggish, in accordance with the lower sensitivity at this operating range. This trend could easily be seen for increasing and decreasing δ.

Figure 15 presents normalized $P_{cav,lpf}$ response to step changes from zero to gradually increasing δ. The 0-deg (not deflected) jet

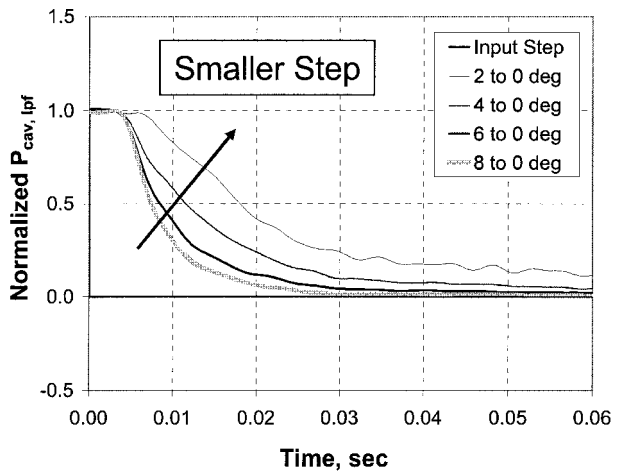

Fig. 16 Closed-loop jet deflection step response δ decreasing to zero (inverted $P_{cav,lpf}$).

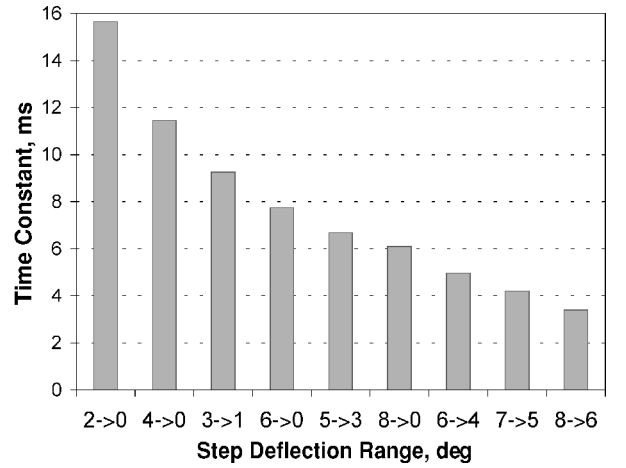

Fig. 17 Closed-loop step response time constants for decreasing jet deflection angles.

angle is a problematic setpoint because the sensitivity at this point is very low. Indeed, when transitioning between $\delta = 0$ and 2 deg, the response is sluggish and accompanied by a steady-state error. As the deflection range increases, the response is faster, and for the low-to-high transitions, it is associated with an increasing overshoot. Note that the high-to-low transitions (steps terminating at $\delta = 0$ deg, the uncontrolled, natural state) are inherently different from the low-to-high transitions (Fig. 16). Physically, this finding can be interpreted as follows. The jet has to be forced to change its natural state. Currently, this is achieved by introducing the periodic excitation at one-quarter of the jet circumference only (Figs. 1a and 1b). Therefore, the only restoring force is the tendency of the jet to return to its uncontrolled state. This difference in the forced pull vs natural restore responses is clearly illustrated by considering the $P_{cav,lpf}$ (Figs. 15 and 16).

An analysis of the time constants of the high-to-low transitions was conducted. It utilized the fact that the natural logarithm of the exponential decay of the jet deflection back to its natural state is linear. Figure 17 presents the calculated time constants for all of the step changes measured, either returning to zero or to a different, but smaller, δ. It was found that the time constants decrease as $\bar{\delta}$ increases, in agreement with the higher static sensitivity of $P_{cav,lpf}$ to δ.

These time constants, multiplied by three, represent the time it takes a first-order system to reach 95% of its final state. This happens between 10 and 45 ms after the command for the highest and lowest $\bar{\delta}$, respectively, corresponding to bandwidths of 50 and 10 Hz. We suppose that this type of response can be altered by using a push–pull controller utilizing two actuators, each situated on an opposite

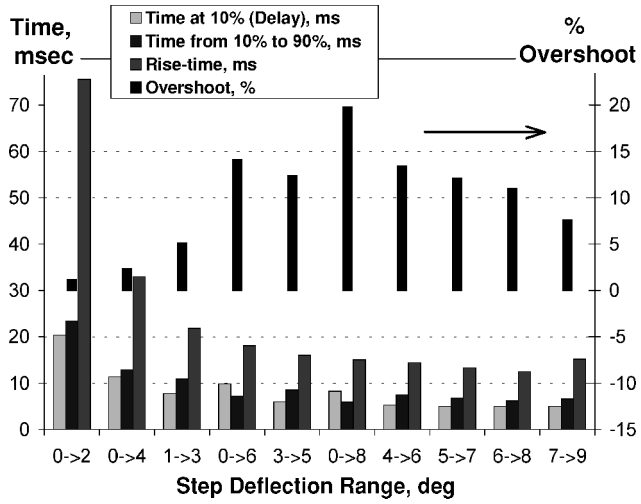

Fig. 18 Closed-loop step response characteristics for increasing δ; step size indicated in abscissa; overshoot in percent of normalized step, with ordinate on right-hand side.

side of the jet centerline, instead of the pull–release mode used throughout this investigation.

Figure 18 presents features of the transient $P_{\text{cav,lpf}}$ response to low-to-high transitions in the δ command. The time lag between the command and the time $P_{\text{cav,lpf}}$ signal increases beyond 10% of the setpoint (delay) is typically 5 ms, close to the design point. It increases to about 10 ms for large step changes and low δ. For $\delta = 0$–2 deg, the delay increases to 20 ms. The time it takes the response to increase from 10 to 90% of the setpoint is about 5–7 ms (Fig. 18). This interval increases in a similar manner to the lag time for small $\bar{\delta}$ (2 deg and smaller). Figure 18 also shows the rise time (the time it takes the plant to cross the setpoint, measured from the command). For the majority of the tested cases (with the exception of those with $\bar{\delta} \leq 2$ deg), the system crosses the setpoint within 12–18 ms from the command. Whether these intervals are sufficiently short or not remains for the applicator to determine. The response overshoot (Fig. 18) is lower than 15% of the setpoint, except for the large 0–8 deg step that reaches 20%.

Overall, the controller performed well near its design point. Outside the linear region, the response became sluggish for small step changes, especially near zero. Whether these performances are sufficient or not is an open question. If there is an application that needs better off-design closed-loop performance, then alternative control methods should be considered. Robustness was not an issue at the onset, and a possible tradeoff may take place between controller complexity and robustness without having to sacrifice the performance at design conditions. Possible robust strategies include linear approaches[19] and nonlinear approaches such as artificial neural networks and fuzzy logic.

IV. Conclusions

Closed-loop control of jet vectoring due to the introduction of periodic excitation over a quarter of the circumference at the junction between the exit from a circular jet and the entrance to a short, wide-angle diffuser was demonstrated experimentally. Detailed static and dynamic identification tests revealed that a single pressure sensor located in the actuator's cavity can be used as the control authority indicator (input), whereas its low-pass filtered signal may serve as a jet deflection indicator (output). This is because the static pressure at the jet–diffuser junction is reduced as the flow turning angle increases. It was demonstrated that the piezoactuator currently used to vector the jet can reach steady state within a few milliseconds from the command, but this rate is too fast compared to the jet response time constant and may, therefore, cause undesirable transient response. Thereafter, the system was modeled, including its typical inverse response. Several linear closed-loop controllers were designed, simulated, and implemented on the plant. It was found that IMC provided an adequate, yet simple, tool for controlling smoothly and rapidly the jet deflection angle. Closed-loop bandwidth was 50 Hz, and the performance of the IMC controller over the entire available range of jet deflection angles was evaluated and shown to perform reasonably well.

Acknowledgments

The experiments were performed at the Steve and Mary Meadow Aerodynamics Laboratory. Partial funding by the Israel Science Foundation, the Fleischman family fund, and the Meadow and Lazarus funds is gratefully acknowledged.

References

[1]Davis, M. R., "Variable Control of Jet Decay," *AIAA Journal*, Vol. 20, No. 5, 1981, pp. 606–609.

[2]Strykowski, P. J., and Wilcoxin, P. J., "Mixing Enhancement Due to Global Oscillations in Jets with Annular Counterflow," *AIAA Journal*, Vol. 31, No. 3, 1993, pp. 564–570.

[3]Strykowski, P. J., and Krothapalli, A., "The Countercurrent Mixing Layer: Strategies for Shear Layer Control," AIAA Paper 93-3260, July 1993.

[4]Strykowski, P. J., Krothapalli, A., and Forliti, D. J., "Counterflow Thrust Vectoring of Supersonic Jets," *AIAA Journal*, AIAA Paper 96-0115, Vol. 34, No. 11, 1996, pp. 2306–2314.

[5]Raman, G., and Cornelius, D., "Jet Mixing Control Using Excitation from Miniature Oscillating Jet," *AIAA Journal*, Vol. 33, No. 2, 1995, pp. 365–368.

[6]Smith, B. L., and Glezer, A., "Vectoring and Small-Scale Motions Effected in Free Shear Flows Using Synthetic Jet Actuators," AIAA Paper 97-0213, Jan. 1997.

[7]Smith, B. L., and Glezer, A., "The Formation and Evolution of Synthetic Jets," *Physics of Fluids*, Vol. 10, No. 9, 1998, pp. 2281–2297.

[8]Crow, S. C., and Champagne, F. H., "Orderly Structure in Jet Turbulence," *Journal of Fluid Mechanics*, Vol. 48, Pt. 3, 1971, pp. 547–591.

[9]Zaman, K. B. M. Q., and Hussain, A. K. M. F., "Turbulence Suppression in Free Shear Flows by Controlled Excitation," *Journal of Fluid Mechanics*, Vol. 103, 1981, pp. 133–159.

[10]Seifert, A., Bachar, T., Koss, D., Shepshelovich, M., and Wygnanski, I., "Oscillatory Blowing, a Tool to Delay Boundary-Layer Separation," *AIAA Journal*, Vol. 31, No. 11, 1993, pp. 2052–2060.

[11]Seifert, A., Darabi, A., and Wygnanski, I., "On the Delay of Airfoil Stall by Periodic Excitation," *Journal of Aircraft*, Vol. 33, No. 4, 1996, pp. 691–699.

[12]Seifert, A., and Wygnanski, I., "Apparatus and Method for Controlling the Motion of a Solid Body or Fluid Stream," Israeli Patent 116668, Submitted 1 Jan. 1996, Granted 6 Dec. 1998 (U.S. Patent granted 26 June 2001), European patent pending.

[13]Pack, L. G., and Seifert, A., "Periodic Excitation for Jet Vectoring and Enhanced Spreading," *Journal of Aircraft*, Vol. 38, No. 3, 2001, pp. 486–495.

[14]Amitay, M., Smith, D. R., Kibens, V., Parekh, D. E., and Glezer, A., 2001. "Aerodynamic Flow Control over an Unconventional Airfoil Using Synthetic Jet Actuators," *AIAA Journal*, Vol. 39, No. 3, 2001, pp. 361–370.

[15]Darabi, A., "On the Mechanisms of Forced Flow Reattachment," Faculty of Engineering, Ph.D. Dissertation, Tel-Aviv Univ., Tel-Aviv, June 2001.

[16]Rapoport, D., Fono, I., Cohen, K., and Seifert, A., "Closed-Loop Vectoring Control of a Turbulent Jet Using Periodic Excitation," AIAA Paper 2002-3073, June 2002.

[17]Dorf, R. C., and Bishof, R. H., *Modern Control Systems*, 7th ed., Addison–Wesley, New York, 1995, p. 404.

[18]Morari, M., and Zafiriou, E., *Robust Process Control*, Prentice–Hall, Englewood Cliffs, NJ, 1989.

[19]Barbu, V., and Sritharan, S. S., "H∞-Control Theory of Fluid Dynamics," *Proceedings of the Royal Society of London*, Vol. 454, 1998, pp. 3009–3033.